Applied Physics Letters

MOCVD growth of InP-based 1.3 μm quantum dash lasers on (001) Si

Cite as: Appl. Phys. Lett. **116**, 142106 (2020); https://doi.org/10.1063/1.5145031
Submitted: 14 January 2020 . Accepted: 15 March 2020 . Published Online: 07 April 2020

Wei Luo, Ying Xue, Bei Shi, Si Zhu, Xu Dong, and Kei May Lau

Applied Physics Letters ARTICLE scitation.org/journal/apl

MOCVD growth of InP-based 1.3 μm quantum dash lasers on (001) Si

Cite as: Appl. Phys. Lett. **116**, 142106 (2020); doi: 10.1063/1.5145031
Submitted: 14 January 2020 · Accepted: 15 March 2020 ·
Published Online: 7 April 2020

View Online Export Citation CrossMark

Wei Luo, Ying Xue, Bei Shi, Si Zhu, Xu Dong, and Kei May Lau[a)]

AFFILIATIONS

Department of Electronic and Computer Engineering, Hong Kong University of Science and Technology, Clear Water Bay, Kowloon, Hong Kong

[a)]**Author to whom correspondence should be addressed:** eekmlau@ust.hk. **Tel.:** (852)23587049. **Fax:** (852) 23581485

ABSTRACT

Quantum dot and quantum dash (QDash) lasers exhibit lower threshold, less temperature sensitivity, and larger modulation bandwidths than the conventional quantum well lasers. For III–V lasers monolithically grown on Si, the stronger carrier confinement and the discrete distribution of these three-dimensional (3D) quantum structures add to their immunity to material defects resulted from hetero-epitaxy. In this study, we report InAs/InAlGaAs/InP QDash lasers emitting at 1.3 μm directly grown on compliant InP/Si substrates by metalorganic chemical vapor deposition. Room-temperature lasing has been demonstrated on both nano-V-groove patterned and unpatterned planar (001) Si under pulsed electrical pumping, with a low threshold current density of 1.05 kA/cm^2. A comparison of lasers grown on these two categories of InP/Si templates in terms of material quality and device performance is presented. Results presented in this work demonstrate the possibility of integrating both datacom and telecom lasers on Si, using the same InAs/InP quantum dash material system on a developed InP-on-Si virtual substrate.

Silicon photonics (SiPh) is a promising technology to address the increasing demand for large-capacity data communication in conjunction with CMOS circuits.[1] Direct epitaxy of III–V materials on silicon enables low-cost and high-volume production of photonic devices, which are potentially compatible with CMOS processes for monolithic integrations.[2] Recently, Si-based photodetectors, (de)multiplexers, and splitters[3–5] have been demonstrated, while an efficient and reliable laser on Si has been under intensive development. Specifically, the defects propagated to the active layers may lead to an increased lasing threshold and rapid device degradation.[6] To address this issue, III–V-on-Si templates of high crystalline quality are needed. Several growth techniques for defect reduction including aspect ratio trapping (ART), thermal cycle annealing (TCA), and strain layer superlattices (SLSs) insertion have been shown to be effective.[7,8] Because of the 3D carrier localization, quantum dots (QDs) and quantum dashes (QDashes) are less sensitive to these defects and have been proven more reliable than quantum wells (QWs).[9] Additionally, the high-temperature stability characteristics of QD or QDash lasers due to the δ-function density states have been experimentally demonstrated.[10]

Using these defect-trapping techniques and 3D quantum structures as gain elements, 1.3 μm InAs/GaAs QD lasers grown on Si by MBE have delivered notable progress, with the lasing threshold current as low as tens of milliampere.[11,12] However, it is challenging to extend the emitting wavelength to the C-band for InAs/GaAs QD due to the large strain inside the active area and weaker carrier confinement.[13] Previously, we have demonstrated both optically pumped and electrically injected 1.5 μm QD and QDash lasers on Si by metalorganic chemical vapor deposition (MOCVD).[14,15] It would be more alluring to cover both the 1.3 and 1.5 μm bands by adopting the InAs/InAlGaAs QDash in the same material system. Based on this paradigm, we report here the InP-based room-temperature electrically pumped 1.3 μm InAs/InAlGaAs QDash lasers grown on on-axis (001) silicon. The emission wavelength can be widely tuned by varying the growth parameters of the InAs QDashes in the MOCVD growth process.

Compared to GaAs grown on Si, a higher density of defects appears in the InP buffer due to a larger lattice mismatch between InP and Si (8%).[16] A GaAs intermediate buffer has been proven effective to obtain a less defective InP-on-Si template with a smooth surface.[17] Furthermore, the material quality and surface roughness of the GaAs layer would inherently affect the defect density and morphology of the InP buffer following. Therefore, to confirm the impact of the GaAs intermediate layer on the final laser characteristics, two kinds of InP/GaAs/Si virtual substrates were developed here, differing from each other in the GaAs-on-Si growth methodologies. In the coalescence of GaAs films on V-groove patterned Si (GoVS),[18] defects generated at the GaAs-Si interface are effectively trapped. For comparison, we also used GaAs on unpatterned (001) Si (GoPS) developed in the past, without the need of nm-scale patterning.[19] On top of the InP-on-Si (IoS) template, a laser structure comprising of three periods InAs/InAlGaAs QDashes was subsequently grown. Preliminary results have revealed that the lasers grown on InP/GoVS exhibited lower threshold current densities than those grown on InP/GoPS templates.

The complete InAs/InAlGaAs QDash laser structure, as well as the InP/GoVS and InP/GoPS templates, was grown in a low-pressure MOCVD system (AIX-200/4). Details of the GoVS growth are available in Ref. 18. Additional defect reduction techniques include five cycles of TCA between 800 °C and 300 °C after 1 μm high-temperature (HT)-GaAs grown at 600 °C. Two periods of $In_{0.16}Ga_{0.84}As$/GaAs SLSs were inserted in the GaAs layer and the final GaAs thickness of the GoVS was 2 μm. For the GoPS growth, the low-temperature (LT)-GaAs was directly grown on unpatterned planar (001) silicon, followed by the same growth procedure of middle-temperature (MT)-GaAs, HT-GaAs, and four cycles of TCA. The total thickness of the GaAs on planar silicon was 1.1 μm.

On top of the GoVS and GoPS templates, 3.1 μm InP was grown with three sets of 10-period $In_{0.61}Ga_{0.39}As$ (12 nm)/InP (34 nm) SLSs inserted to repulse and filter the TDs.[20] Afterward, 600 and 630 nm of Si-doped InP were grown as n-contact and n-cladding layers, respectively, followed by three layers of InAs/InAlGaAs QDashes as the gain elements. The doping concentrations of the n-contact and n-cladding layer were calibrated to be 5×10^{18} cm^{-3} and 5.5×10^{17} cm^{-3}, respectively. Finally, a 1.65 μm-thick zinc-doped InP p-cladding layer as well as a 140 nm $In_{0.515}Ga_{0.485}As$ p-contact layer was grown sequentially with a doping concentration of 9×10^{17} cm^{-3} and 1.6×10^{19} cm^{-3}, respectively. The complete structure of the fabricated Fabry–Pérot (FP) laser grown on InP/GoVS is shown in Fig. 1(a). The QDashes were grown at a pressure of 100 mbar and a temperature of 510 °C. After the QDash deposition, a 5-s growth interruption was applied for self-assembled QDashes formation.[21] A LT-InAlGaAs layer was then grown at the same temperature to prevent desorption of the QDashes. The temperature was ramped up to 630 °C and a HT-InAlGaAs spacer was grown. The whole active region was sandwiched by additional HT-InAlGaAs layers to form a separate confinement heterostructure (SCH), along with thick InP claddings to provide essential optical confinement.[22]

The as-grown samples were processed into ridge waveguide FP lasers with the cavity width varied from 2 μm to 70 μm by photolithography, dry-etching, and metallization.[23] Compared to the double-side contact laser on the n-InP substrate, the QDash lasers on silicon were processed via "top–top" contacts to prevent the current flow through the defective buffer layers and the III–V/Si interface, leading to carrier scattering and non-radiative recombination. The substrate was finally thinned down to about 100 μm and subsequently cleaved into laser bars with lengths varying from 0.5 mm to 2 mm without any facet coatings. A color-enhanced cross section SEM image of an as-fabricated laser (ridge width = 8 μm) is shown in Fig. 1(b) with a clean and mirror-like facet, minimizing the cavity loss.

The quality of the IoS templates and the optical properties of the QDashes are two crucial aspects to be optimized for desirable laser performance. Instead of using 4–6° offcut silicon substrates to eliminate the anti-phase boundaries (APBs),[24–26] we grew III–V layers on V-grooved Si or nominal on-axis (001) silicon. Approximately 30 min of annealing at 800 °C was performed before III–V growth to form double-atomic terraces, which helps the self-annihilation of APBs during GaAs growth.[27] The surface roughness values (root mean square (RMS)) of InP/GoPS and InP/GoVS were 3.7 nm and 1.5 nm, respectively, across a 10×10 μm^2 scanning area [Figs. 2(a) and 2(b)]. To examine the effect of InGaAs/InP SLSs inserted in the InP buffer, an XTEM sample of an InAs QDash laser grown on the InP/GoVS template was prepared by focused ion beam (FIB). Figure 3(a) shows that many defects introduced at the GaAs/InP interface were well trapped by three periods of SLSs, and less defective InP layer was, thus, obtained above the SLSs. Based on statistical sampling of plan-view TEM images, the defect densities on InP/GoVS and InP/GoPS are counted to be 2.75×10^8 cm^{-2} and 3.54×10^8 cm^{-2}, respectively.

A smooth InP buffer is a prerequisite to minimize the inhomogeneous broadening of QDashes. Before the QDash growth, a 1.3-nm-thick InGaAs was grown to manage the strain of the QDashes and control its shape and density.[28] By changing the indium composition of the InGaAs layer, the bandgap of the dot-in-well (DWELL) structure and the QDash current injection efficiency can be tailored.[29] Moreover, the double InAlGaAs cap layer was grown to avoid QDash desorption at high temperatures and to control the height of the QDashes by strain compensation.[30–32] To increase the QDash density, 3-layer vertically stacked QDashes were grown and separated by 30 nm InAlGaAs spacers.[33] Figure 3(b) demonstrates that the

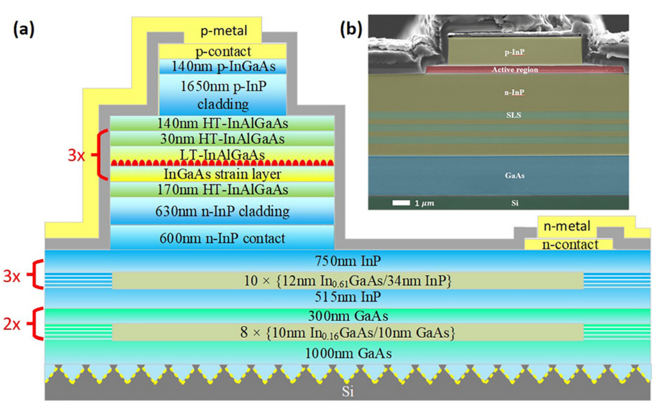

FIG. 1. (a) Schematic of the fabricated InAs/InAlGaAs QDash laser device on V-grooved Si including the detailed structure parameters of the QDash active region and InP buffer (not to scale); (b) color-enhanced SEM image of a fabricated Fabry–Pérot laser device with mirror-like facet.

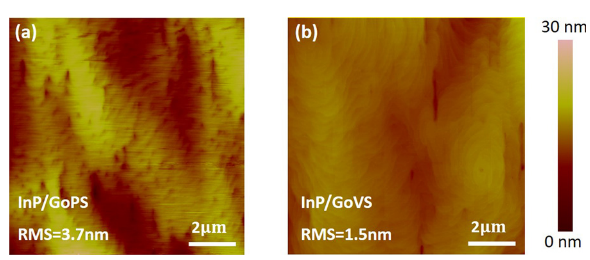

FIG. 2. 10×10 μm^2 AFM images of the (a) InP/GoPS and (b) InP/GoVS templates after 3.1 μm InP growth, with RMS value of 3.7 nm and 1.5 nm, respectively.

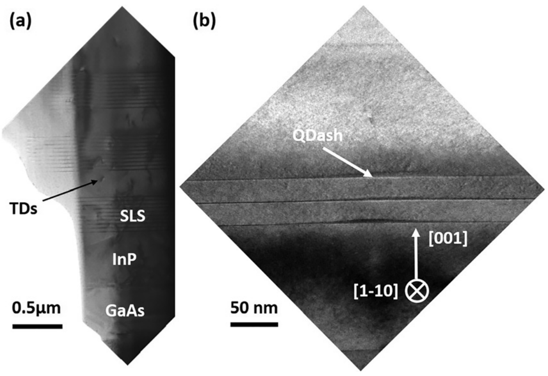

FIG. 3. (a) Cross-sectional TEM of the SLS inserted in the InP layer grown on GoVS; (b) zoomed-in TEM of 3-layer stacking InAs QDash grown on InP/GoVS with an InAlGaAs spacer observed from the [1-10] direction.

three-layer QDashes are vertically aligned due to an accumulated strain field. The QDash density was estimated to be $2.5 \times 10^{10}\,\mathrm{cm}^{-2}$ based on the AFM image [Fig. 4(a)], and the QDashes were aligned along the [1-10] direction.

The deposition amount of QDashes plays the most important role in tuning the emission wavelength. A significant blue-shift was observed when reducing the deposition amount from 2.4 monolayer (ML) to 1.6 ML as shown in Fig. 4(b). The wavelength tuning was mainly attributed to the shrinkage of QDash geometries.[34] Figure 4(c) presents the room temperature PL spectra of QDashes grown on InP/GoPS and InP/GoVS templates in the same batch. The peak wavelength of the QDashes on InP/GoVS is approximately 45 nm red-shifted compared to those on InP/GoPS. The wavelength discrepancy is speculated to be related to the different residual strain and surface temperature of the two templates. Even though the PL intensity of the QDashes grown on InP/GoVS was lower than that grown on InP/GoPS shown in Fig. 4(c), the devices fabricated on InP/GoVS exhibited lower thresholds. This is primarily because the QDash growth condition was initially optimized on InP/GoPS instead of on InP/GoVS, resulting in a weaker PL intensity for QDashes on InP/GoVS. However, the material quality, regarding defect density and surface roughness, of the InP/GoVS accounts for the more appealing device result.[6] With further optimization of QDash growth condition on InP/GoVS, PL performance will be improved, and continuous-wave lasing of the fabricated devices can be anticipated.

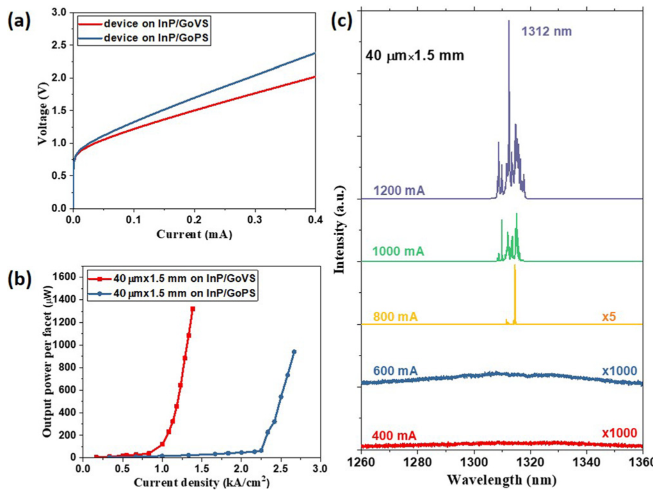

FIG. 5. (a) I-V curves of different size InAs QDash lasers grown on InP/GoVS and InP/GoPS; (b) L–I curves of $40\,\mu m \times 1.5$ mm InAs QDash lasers grown on InP/GoVS and InP/GoPS; (c) emission spectrum of a $40\,\mu m \times 1.5$ mm InAs QDash laser grown on InP/GoVS under pulsed current injection at room temperature.

The cleaved FP laser bars were measured at room temperature under pulsed current injection with a 0.5% duty cycle and 400 ns pulse width. Series resistances between 2 and 8 Ω are obtained from typical device I-V curves as shown in Fig. 5(a). The light–current (L–I) curves of $40\,\mu m \times 1.5$ mm lasers on InP/GoVS and InP/GoPS are shown in Fig. 5(b). The lowest threshold current density, 1.05 kA/cm^2, was achieved on the InP/GoVS template. The single facet output power of a $20\,\mu m \times 1$ mm laser on InP/GoVS reaches 22 mW without roll-over. Among the lasers grown on InP/GoPS, the lowest threshold current density measured was 2.24 kA/cm^2 for a $40\,\mu m \times 1.5$ mm device. This result suggests a lower defect density of the InP buffer grown on GoVS. The electroluminescence (EL) spectrum of a $40\,\mu m \times 1.5$ mm QDash laser grown on InP/GoVS under pulsed current injection at room temperature is shown in Fig. 5(c). Multimode lasing occurs at the progressively increasing current levels. The dependence of threshold current densities on the cavity lengths are plotted in Fig. 6(a).

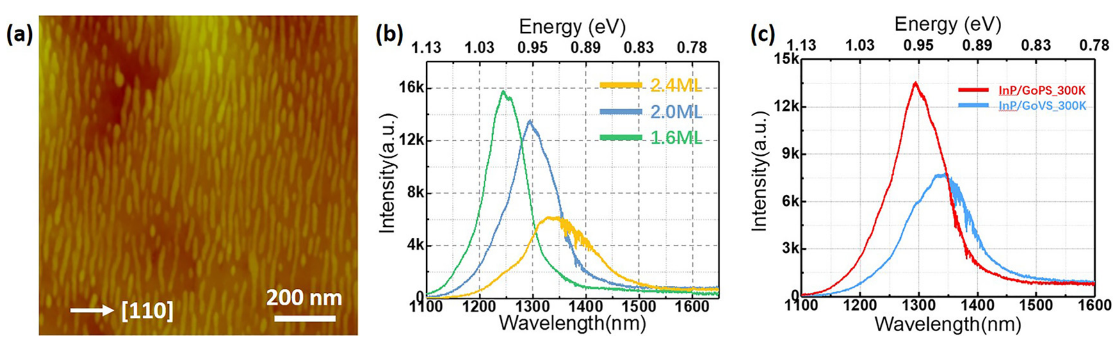

FIG. 4. (a) $1 \times 1\,\mu m^2$ AFM image of the fourth layer QDash grown on InP/GoVS without capping for calibration; (b) room temperature PL of QDashes with different deposition amounts grown on InP/GoPS templates; (c) room temperature PL of QDashes grown on InP/GoPS and InP/GoVS templates.

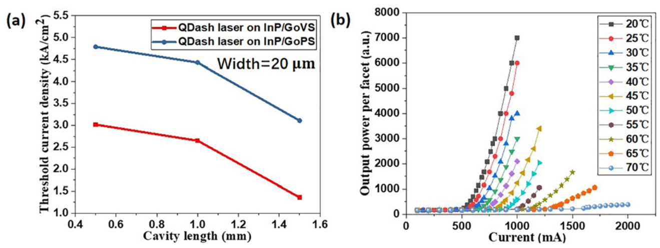

FIG. 6. (a) Threshold current densities of InAs QDash lasers grown separately on InP/GoVS and InP/GoPS with 20 μm cavity width and different cavity lengths; (b) light output power vs current of a 20 μm × 1.5 mm InAs QDash laser grown on InP/GoPS at different temperatures.

Generally, devices with longer cavities exhibit a lower threshold current density on both InP/GoPS and InP/GoVS due to a higher net gain to overcome the optical losses.

The temperature-dependent L-I curves of a 20 μm × 1.5 mm InAs/InAlGaAs QDash laser grown on InP/GoPS are shown in Fig. 6(b). The laser can operate up to 70 °C with a characteristic temperature T_0 of 49 K. Similar results were attained for QDash lasers on InP/GoVS. The 1.3 μm InAs QDash lasers grown on IoS by MOCVD presented in this work are comparable to the reports of 1.3 μm InAs QD lasers grown on GaAs-on-Si by molecular beam epitaxy (MBE).[24,35] In addition to optimizing the InP buffer grown on Si to reduce nonradiative recombinations, the QDashes uniformity can be further improved. The indium composition of the InGaAs/InP SLS can be increased to further reduce the threading dislocations with larger strain.[36]

In conclusion, we have demonstrated the all MOCVD-grown InP-based electrically pumped 1.3 μm InAs/InAlGaAs QDash lasers on on-axis (001) silicon. The emission wavelength of InAs/InAlGaAs QDashes can cover both 1.3 and 1.5 μm bands by tuning the growth parameters of QDashes. The combined dislocation filtering techniques provide a better IoS buffer with fewer defects, leading to a threshold current density as low as ~1.05 kA/cm^2 under room temperature pulse operations, and a characteristic temperature of 47 K for lasers implemented on InP/GoVS buffer. Without the need of nano-patterned Si substrate, electrically pumped lasers grown on InP/GoPS also lase with a higher threshold current ~2.24 kA/cm^2. Therefore, this platform offers a feasible path toward achieving O-band and C-band lasers using the same InP-based material system by the manufacturing-friendly MOCVD process, benefiting Si-based on-chip optical interconnects. Compared to the recent high-quality GaAs on Si with defect density on the order of 10^6 cm^{-2}, InP on Si used here is still on the order of 10^8 cm^{-2}. With future improvement of the material quality of InP on Si by optimizing the SLS and strain engineering to accommodate the lattice mismatch, continuous-wave lasing of InP-based QDash lasers can be anticipated.

See the supplementary material for the SEM image of the cleaved laser facet without color enhancement and L–I curves of the 2 mm-long lasers on InP/GoPS and InP/GoVS.

AUTHORS' CONTRIBUTIONS

W.L. and Y.X. contributed equally to this work.

This work was supported in part by Research Grants Council of Hong Kong (Nos. 614813 and 16212115) and in part by the Innovation and Technology Fund of Hong Kong (No. ITS/273/16FP). The author would like to thank Nanosystem Fabrication Facility (NFF) and Material Characterization & Preparation Facility (MCPF) of HKUST for their technical support and discussion, Zhao Yan, Jie Huang, and Chak Wah Tang for growth discussion, and Dr. Yu Han for helpful discussion and characterization guidance.

REFERENCES

[1]D. Thomson, A. Zilkie, J. E. Bowers, T. Komljenovic, G. T. Reed, L. Vivien, D. Marris-Morini, E. Cassan, L. Virot, J.-M. Fédéli, J.-M. Hartmann, J. H. Schmid, D.-X. Xu, F. Boeuf, P. O'Brien, G. Z. Mashanovich, and M. Nedeljkovic, J. Opt. **18**, 073003 (2016).
[2]S. Chen, W. Li, J. Wu, Q. Jiang, M. Tang, S. Shutts, S. N. Elliott, A. Sobiesierski, A. J. Seeds, I. Ross, P. M. Smowton, and H. Liu, Nat. Photonics **10**, 307 (2016).
[3]B. W. Jia, K. H. Tan, W. K. Loke, S. Wicaksono, K. H. Lee, and S. F. Yoon, ACS Photonics **5**, 1512 (2018).
[4]J. Wang and L. R. Chen, Opt. Express **23**, 26450 (2015).
[5]H. Wu, Y. Tan, and D. Dai, Opt. Express **25**, 6069 (2017).
[6]D. Jung, R. Herrick, J. Norman, K. Turnlund, C. Jan, K. Feng, A. C. Gossard, and J. E. Bowers, Appl. Phys. Lett. **112**, 153507 (2018).
[7]Q. Li and K. M. Lau, Prog. Cryst. Growth Charact. Mater. **63**, 105 (2017).
[8]L. Megalini, S. Šuran Brunelli, W. Charles, A. Taylor, B. Isaac, J. Bowers, and J. Klamkin, Materials **11**, 337 (2018).
[9]R. Beanland, A. M. Sánchez, D. Childs, K. M. Groom, H. Y. Liu, D. J. Mowbray, and M. Hopkinson, J. Appl. Phys. **103**, 014913 (2008).
[10]M. V. Maximov, A. F. Tsatsul'nikov, B. V. Volovik, D. S. Sizov, Y. M. Shernyakov, I. N. Kaiander, A. E. Zhukov, A. R. Kovsh, S. S. Mikhrin, V. M. Ustinov, Z. I. Alferov, R. Heitz, V. A. Shchukin, N. N. Ledentsov, D. Bimberg, Y. G. Musikhin, and W. Neumann, Phys. Rev. B **62**, 16671 (2000).
[11]D. Jung, J. Norman, M. J. Kennedy, C. Shang, B. Shin, Y. Wan, A. C. Gossard, and J. E. Bowers, Appl. Phys. Lett. **111**, 122107 (2017).
[12]J. Kwoen, B. Jang, K. Watanabe, and Y. Arakawa, Opt. Express **27**, 2681 (2019).
[13]S. Bhowmick, M. Z. Baten, T. Frost, B. S. Ooi, and P. Bhattacharya, IEEE J. Quantum Electron. **50**, 7 (2014).
[14]B. Shi, S. Zhu, Q. Li, Y. Wan, E. L. Hu, and K. M. Lau, ACS Photonics **4**, 204 (2017).
[15]S. Zhu, B. Shi, Q. Li, and K. M. Lau, Appl. Phys. Lett. **113**, 221103 (2018).
[16]T. Orzali, A. Vert, B. O'Brien, J. L. Herman, S. Vivekanand, R. J. W. Hill, Z. Karim, and S. S. Papa Rao, J. Appl. Phys. **118**, 105307 (2015).
[17]Y. Kohama, Y. Kadota, and Y. Ohmachi, Jpn. J. Appl. Phys., Part 1 **28**, 1337 (1989).
[18]Q. Li, K. W. Ng, and K. M. Lau, Appl. Phys. Lett. **106**, 072105 (2015).
[19]M. Li, H. Li, C. W. Tang, and K. M. Lau, IEEE Electron Device Lett. **33**, 498 (2012).
[20]D. Jung, P. G. Callahan, B. Shin, K. Mukherjee, A. C. Gossard, and J. E. Bowers, J. Appl. Phys. **122**, 225703 (2017).
[21]B. Tongbram, A. Ahmad, S. Sengupta, A. Mandal, J. Singhal, A. Balgarkashi, and S. Chakrabarti, J. Lumin. **192**, 89 (2017).
[22]Z. Y. Zhang, A. E. H. Oehler, B. Resan, S. Kurmulis, K. J. Zhou, Q. Wang, M. Mangold, T. Süedmeyer, U. Keller, K. J. Weingarten, and R. A. Hogg, Sci. Rep. **2**, 477 (2012).
[23]S. Zhu, B. Shi, Q. Li, and K. M. Lau, Opt. Express **26**, 14514 (2018).
[24]T. Wang, H. Liu, A. Lee, F. Pozzi, and A. Seeds, Opt. Express **19**, 11381 (2011).
[25]J. R. Orchard, S. Shutts, A. Sobiesierski, J. Wu, M. Tang, S. Chen, Q. Jiang, S. Elliott, R. Beanland, H. Liu, P. M. Smowton, and D. J. Mowbray, Opt. Express **24**, 6196 (2016).
[26]Z. Huang, M. Zimmer, S. Hepp, M. Jetter, and P. Michler, IEEE J. Quantum Electron. **55**, 1 (2019).
[27]B. Kunert, I. Németh, S. Reinhard, K. Volz, and W. Stolz, Thin Solid Films **517**, 140 (2008).

[28]K. Akahane, N. Ohtani, Y. Okada, and M. Kawabe, J. Cryst. Growth **245**, 31 (2002).
[29]J. Tatebayashi, M. Nishioka, and Y. Arakawa, Appl. Phys. Lett. **78**, 3469 (2001).
[30]F. Ferdos, S. Wang, Y. Wei, A. Larsson, M. Sadeghi, and Q. Zhao, Appl. Phys. Lett. **81**, 1195 (2002).
[31]K. Akahane, N. Yamamoto, and T. Kawanishi, Phys. Status Solidi A **208**, 425 (2011).
[32]B. Shi and K. M. Lau, J. Cryst. Growth **433**, 19 (2016).
[33]J. O. Kim, S. Sengupta, A. V. Barve, Y. D. Sharma, S. Adhikary, S. J. Lee, S. K. Noh, M. S. Allen, J. W. Allen, S. Chakrabarti, and S. Krishna, Appl. Phys. Lett. **102**, 011131 (2013).
[34]A. Sauerwald, T. Kümmell, G. Bacher, A. Somers, R. Schwertberger, J. P. Reithmaier, and A. Forchel, Appl. Phys. Lett. **86**, 253112 (2005).
[35]J. Kwoen, B. Jang, J. Lee, T. Kageyama, K. Watanabe, and Y. Arakawa, Opt. Express **26**, 11568 (2018).
[36]A. Watanabe, J. J. Freedsman, R. Oda, T. Ito, and T. Egawa, Appl. Phys. Express **7**, 041002 (2014).